ORIGINAL PAPER

# Synthesis and characterization of $Fe_3O_4$@$SiO_2$–polymer-imid–Pd magnetic porous nanospheres and their application as a novel recyclable catalyst for Sonogashira–Hagihara coupling reactions

Esmaeilpour Mohsen · Javidi Jaber · Mokhtari Abarghoui Mehdi · Nowroozi Dodeji Fatemeh

**Abstract** We demonstrate herein the modification of magnetic nanoparticles and their use as a magnetic nanocatalyst in direct coupling reactions of aryl halides with terminal alkynes. Magnetite particles were prepared by simple co-precipitation method in aqueous medium, and then $Fe_3O_4$@ $SiO_2$ nanosphere was synthesized by using nano-$Fe_3O_4$ as the core, TEOS as the silica source and PVA as the surfactant. $Fe_3O_4$@$SiO_2$ was coated with polymeric $N$-heterocyclic carbene/Pd. The samples were characterized by X-ray diffraction, Fourier transform infrared spectroscopy, transmission electron microscopy, field emission scanning electron microscopy, dynamic light scattering, thermogravimetric analysis, vibration sample magnetometer and $N_2$ adsorption–desorption isotherm analysis. Poly ($N$-vinyl imidazole) functionalized $Fe_3O_4$@$SiO_2$ nanoparticle was found to be an efficient nanocatalyst in Sonogashira–Hagihara cross-coupling reactions. The nanocatalyst can be easily recovered by a magnetic field and reused for six runs without appreciable loss of its catalytic activity.

E. Mohsen · N. D. Fatemeh
Chemistry Department, College of Science, Shiraz University, Shiraz, Iran
e-mail: m1250m551085@yahoo.com

J. Jaber (✉)
Department of Pharmaceutics, School of Pharmacy, Shaheed Beheshti University of Medical Sciences, Tehran, Iran
e-mail: jaberjavidi@gmail.com

M. A. Mehdi
Department of Chemistry, Isfahan University of Technology, Isfahan, Iran

## Introduction

During the past decade, scientists have developed techniques for synthesizing and characterizing many new materials with at least one dimension on the nanoscale, including nanoparticles, nanolayers and nanotubes [1]. Nanostructured materials, a new branch of materials research, are attracting a great deal of attention because of their potential applications in areas such as catalysis [2], electronics [3], ceramics [4], optic [5], magnetic data storage [6] and nanocomposites. One of the most fundamental characteristics of nanometer-sized particles is their very high surface-to-volume ratio. This can lead to novel and unexpected atomic arrangements and may also have dramatic effects on other physical or chemical attributes [7].

In recent years, the synthesis of superparamagnetic nanoparticles has been intensively developed not only for its fundamental scientific interest, but also for many technological applications: catalytic [8], biosensing [9], magnetic storage media [10], medical applications, such as contrast agents in magnetic resonance imaging (MRI) [11–14], targeted drug delivery [15, 16], magnetic inks for jet printing [17], tissue repairing [18], immunoassay and [18] hyperthermia treatment of cancer cells [19], detoxification of biological fluids [18] and cell separation [18]. These applications are mainly based on the magnetic feature of the solid phase that enables achieving a rapid and easy separation from the reaction medium in a magnetic field [20].

Nanoscale magnetite ($Fe_3O_4$) is cheap, non-toxic, biocompatible and easy to prepare [21]. Many methods have

been developed for the preparation of $Fe_3O_4$ such as sonochemical synthesis [22], thermal decomposition [23], microemulsions [24] and chemical co-precipitation [25, 26]. Among these methods, chemical co-precipitation may be the most promising, because of its simplicity and productivity.

Recently, magnetic core–shell nanostructures have attracted more attention due to their unique magnetic properties. These core–shell nanostructure magnetic catalysts can be easily retrieved under the influence of a magnetic field and used in subsequent reactions. Due to this property, using magnetic core–shell structure composites as catalysts has been recommended in many studies [27]. Also, several methods have been developed to prepare polymer coatings on magnetite nanoparticles such as physical adsorption of polymers and emulsion polymerization in the presence of nanoparticles, the so-called "grafting-to" and "grafting-from" methods [28, 29].

Obviously, homogeneous catalysts show higher catalytic activities than their heterogeneous counterparts because of their solubility in reaction media, which increases catalytic site accessibility for the substrate. However, recycling homogeneous catalysts is often tedious and time consuming and there is also the issue of product contamination observed when these catalysts are used [27]. Immobilization of homogeneous catalysts on various insoluble supports, especially porous materials with high surface areas, is usually the method of choice, since the immobilized catalysts can be facilely recovered via a simple filtration process after reactions [30]. Therefore, a number of functionalized $Fe_3O_4$ nanoparticles have been employed in a range of organic transformations, and several studies on immobilization of metal and organo-catalysts on silica-coated iron oxide nanoparticles have been reported [31–34].

Palladium-catalyzed Sonogashira–Hagihara cross-coupling is one of the most widely used carbon–carbon forming reactions [35, 36] and has been widely applied in areas such as natural products [37], pharmaceuticals [38] and biologically active molecules [39]. It provides an efficient route to obtain materials for nonlinear optical and molecular electronics [40], alkenyl- and arylacetylenes, substituted alkynes [41], conjugated oligomers and polymers [42] and symmetrical diynes [43]. The Sonogashira coupling reaction of terminal alkynes with aryl halides can occur in the presence of catalysts such as MCM-41-S–Pd(0) [44], Pd/C [45], CELL–Pd(0) [46], Pd(dmba)Cl(PTA) [47], $PdCl_2(PCy_3)_2$ [48] and $PdCl_2(PPh_3)_2$ [49]. In addition, the use of transition metals such as Co [50], Fe [51, 52], Ni [53], In [54] and Ru [55] has been also reported for these reactions. Although these methods are valuable, many of these procedures have significant drawbacks such as tedious workup procedures, low yields, long reaction times, high temperatures and non-recoverable catalysts. Thus, the development of a new

procedure for the Pd-catalyzed Sonogashira–Hagihara reaction is still a desirable goal.

In this work, we report the preparation of $Fe_3O_4@SiO_2$–polymer-imid–Pd nanocatalyst as illustrated in Scheme 1 and its use as a magnetic nanocatalyst in direct coupling reactions of aryl halides with terminal alkynes.

## Experimental

### General

All the chemicals reagents used in our experiments were purchased from the Merck Chemical Company in high purity. All the solvents were distilled, dried and purified by standard procedures. Fourier transform infrared (FT-IR) spectra were obtained using a Shimadzu FT-IR 8300 spectrophotometer. NMR spectra were recorded on a Bruker Avance DPX 250 MHz spectrometer in $CDCl_3$ or DMSO-$d_6$ using tetramethylsilane (TMS) as an internal reference. X-ray powder diffraction (XRD) spectra were taken on a Bruker AXS D8-advance X-ray diffractometer with Cu Kα radiation ($\lambda = 1.5418$). Transmission electron microscopy (TEM) images were obtained on a Philips EM208 transmission electron microscope with an accelerating voltage of 100 kV, and field emission scanning electron microscopy (FE-SEM) images were obtained on HITACHI S-4160. The BET surface area and porosity of catalysts were determined from nitrogen physisorption measured on a Micromeritics ASAP 2000 instrument at 196 °C. TGA thermograms were recorded on an instrument of Perkin Elmer with $N_2$ carrier gas and with the rate of temperature change of 20 °C min$^{-1}$. Magnetic properties were obtained on a BHV-55 vibrating sample magnetometer (VSM) and dynamic light scattering (DLS) was recorded on a HORIBA-LB550. Pd loading and leaching test was carried out with an inductively coupled plasma (ICP) analyzer (Varian, vista-pro). Mass spectra were obtained at 70 eV. All products were identified by comparison of their spectral data and physical properties with those of the authentic sample and all yields refer to isolated products. The progress of the reaction was monitored by TLC and purification was achieved by silica gel column chromatography.

### General procedure

#### Preparation of $Fe_3O_4@SiO_2$ core–shell

The core–shell $Fe_3O_4@SiO_2$ nanospheres were prepared by a modified Stober method in our previous work [27]. In a typical procedure, the mixture of $FeCl_3·6H_2O$ (1.3 g, 4.8 mmol) in water (15 mL) was added to the solution of polyvinyl alcohol (PVA 15000), as a surfactant, and
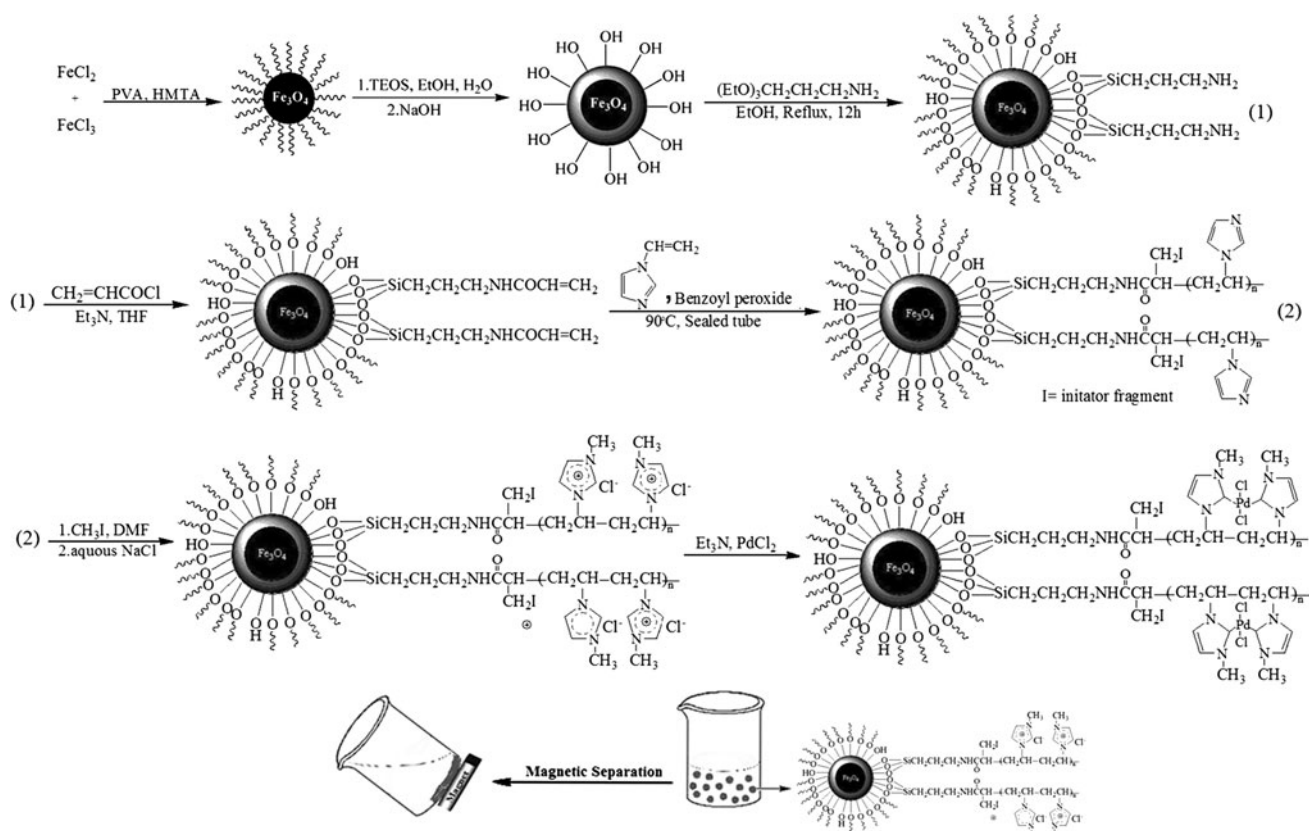
**Scheme 1** Process for preparation of polymeric *N*-heterocyclic carbene/Pd functionalized $Fe_3O_4@SiO_2$ nanoparticle

$FeCl_2 \cdot 4H_2O$ (0.9 g, 4.5 mmol) in water (15 mL), which was prepared by completely dissolving PVA in water followed by addition of $FeCl_2 \cdot 4H_2O$. The resultant solution was left to be stirred for 30 min in 80 °C. Then, hexamethylenetetraamine (HMTA) (1.0 mol/L) was added dropwise with vigorous stirring to produce a black solid product when the reaction media reached pH 10. The resultant mixture was heated on a water bath for 2 h at 60 °C, the black magnetite solid product was filtered and washed with ethanol three times and was then dried at 80 °C for 10 h. Then, $Fe_3O_4$ nanoparticle (0.50 g, 2.1 mmol) was dispersed in the mixture of ethanol (50 mL), deionized water (5 mL) and tetraethoxysilane (TEOS) (0.20 mL), followed by the addition of 5.0 mL of NaOH (10 wt%). This solution was stirred mechanically for 30 min at room temperature. Then the product, $Fe_3O_4@SiO_2$, was separated by an external magnet and was washed with deionized water and ethanol three times and dried at 80 °C for 10 h.

### Synthesis of poly (N-vinylimidazole) functionalized $Fe_3O_4@SiO_2$ nanoparticle (Fe3O4@SiO2–polymer-imid)

$Fe_3O_4@SiO_2$ (1 g) was added to the solution of 3-aminopropyl (triethoxy) silane (1 mmol, 0.176 g) in ethanol (10 mL) and the resultant mixture was kept under reflux for

12 h. The solvent was removed and the resulting solid ($Fe_3O_4@SiO_2$–$NH_2$) was dried at 80 °C overnight. The product was washed with ethanol and water to remove unreacted species and dried at 80 °C for 6 h. $Fe_3O_4@SiO_2$–$NH_2$ (1 g) was suspended in dry THF (15 mL) and the suspension cooled down to 0 °C. Triethylamine (0.151 g, 1.5 mmol) was added, followed by addition of acryloyl chloride (0.109 g, 1.2 mmol) over a period of 1 h. Then, the resultant mixture was stirred at 0 °C for a further 4 h and the modified $Fe_3O_4@SiO_2$ was isolated by external magnetic field and washing with THF (10 mL), water (2 × 10 mL) and acetone (10 mL). The solid obtained was then dried at 80 °C for 12 h. To the resultant mixture (1.0 g), *N*-vinylimidazole (2 mL) and recrystallized benzoyl peroxide (0.025 g) were added and the mixture was heated at 80 °C for 12 h. The poly (*N*-vinylimidazole) functionalized $Fe_3O_4@$-$SiO_2$ nanoparticle (Fe3O4@SiO2–polymer-imid) was separated by an external magnet, washed with deionized water and ethanol three times and dried at 80 °C for 10 h.

### Synthesis of polymer-imid–Pd functionalized $Fe_3O_4@SiO_2$ nanoparticle (Fe3O4@SiO2–polymer-imid–Pd)

Fe3O4@SiO2–polymer-imid (1 g) was dispersed in the DMF solution (15 mL), ultrasonically for 15 min. Then,

methyl iodide (2.5 mmol, 0.155 mL) was added, the mixture was stirred at 80 °C for 16 h and filtered in an external magnetic field. The product was washed with DMF and ethanol to remove any reacted species and dried at 70 °C for 6 h. The resultant solid product stirred in NaCl solution (5 %) (30 mL) at room temperature for 24 h. The mixture was filtered off, washed thoroughly with excess $H_2O$ and then dried in an oven under vacuum at 70 °C for 8 h (Fe3O4@SiO2–polymer-imid–S). The chloride ion capacity of imidazolium-type $Fe_3O_4$@$SiO_2$-polymer was found using an argentometric titration method (0.1 g of Fe3O4@SiO2–polymer-imid–S was suspended in 10 mL of 0.1 M $HNO_3$. After adding 1 mL of 0.1 M $AgNO_3$, the mixture was stirred for 10 h at room temperature. The chloride counterions precipitated as AgCl. The remaining $Ag^+$ was back titrated using 0.1 M HCl. The permanent charge density of imidazole groups was calculated to be 1.31 mmol/g). The resulting Fe3O4@SiO2–polymer-imid–S (1.0 g) was reacted with $PdCl_2$ (3 mmol) in the presence of $Et_3N$ (6 mmol) as a base and DMF (15 mL) as a solvent at 80 °C for 16 h. The mixture (Fe3O4@SiO2–polymer-imid–Pd) was filtered in an external magnetic field, washed thoroughly with DMF (2 × 5 mL) and $H_2O$ (2 × 5 mL) and dried at 70 °C for 8 h.

### General procedure for the Sonogashira–Hagihara reaction using Fe3O4@SiO2–polymer-imid–Pd magnetic nanocatalyst

A mixture of ArX (1.0 mmol), alkyne (1.2 mmol), $Fe_3O_4$@$SiO_2$-polymer-imid–Pd magnetic nanocatalyst (0.03 g), $Et_3N$ (2 mmol) and DMF (4.0 mL) was stirred at 80 °C in an oil bath. The progress of the reaction was monitored by TLC or GC. After completion of the reaction and separation of Fe3O4@SiO2–polymer-imid–Pd using a magnetic field, 15 mL of water was added and the mixture extracted with $Et_2O$. The combined organic phases were washed with water (2 × 5 mL) and dried over anhydrous $Na_2SO_4$. Then, the solvent was removed under reduced pressure. The resulting crude product was purified by flash chromatography to give the desired pure coupling products in high to excellent isolated yields.

### Results and discussion

The FT-IR spectrum of $Fe_3O_4$, $Fe_3O_4$@$SiO_2$, $Fe_3O_4$@$SiO_2$–NH$_2$, Fe3O4@SiO2–polymer-imid, Fe3O4@SiO2–polymer-imid–S and Fe3O4@SiO2–polymer-imid–Pd nanoparticles are shown in Fig. 1a–f. In Fig. 1a, the absorption band at 559 cm$^{-1}$ is assigned to the stretching vibration of the Fe–O band of $Fe_3O_4$. Also, the peaks at around 3,400 and 1,620 cm$^{-1}$ in Fig. 1a are due to the adsorbed water in the
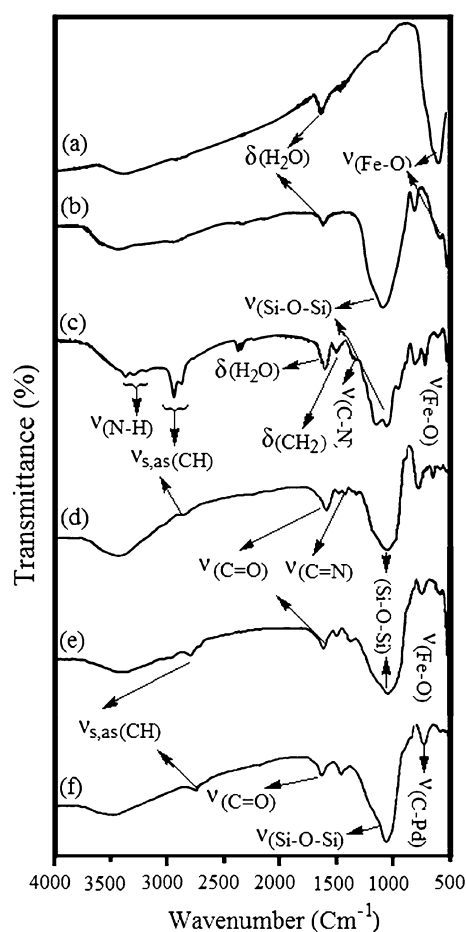


**Fig. 1** FT-IR spectra: *a* $Fe_3O_4$, *b* $Fe_3O_4$@$SiO_2$, *c* $Fe_3O_4$@$SiO_2$–NH$_2$, *d* Fe3O4@SiO2–polymer-imid, *e* Fe3O4@SiO2–polymer-imid-S and Fe3O4@SiO2–polymer-imid–Pd

sample. The surfaces of pure $Fe_3O_4$ nanoparticles were readily covered with $SiO_2$ layers. In Fig. 1b, the presence of vibration bands at 561, 1,000–1,150 and 3,400 cm$^{-1}$, due to Fe–O, Si–O–Si, and –OH, respectively, demonstrates the existence of $Fe_3O_4$@ $SiO_2$. Figure 1c shows the FT-IR spectrum of $Fe_3O_4$@$SiO_2$–NH$_2$ nanoparticles; the peaks at 560, 1,000–1,150, 1,400–1,410 and 1,543 cm$^{-1}$ are attributed to Fe–O (stretching vibration), Si–O–Si (asymmetric stretching), C–N(stretching vibration) and N–H (bending), respectively. Also, the presence of several bands with medium intensity in 28,010–2,986 cm$^{-1}$ and 3,050–3,250 regions are allocated to C–H stretching of the propyl group and N–H stretching (Fig. 1c). The presence of vibration bands at 559, 1,000–1,150, 1,445, 1,649 and 2,792–2,985, due to Fe–O, Si–O–Si, C=N, C=O and CH, respectively, demonstrates the existence of $Fe_3O_4$@$SiO_2$–polymer-imid in the spectrum (Fig. 1d). The FT-IR spectrum of Fe3O4@SiO2–polymer-imid–S exhibits a band at 1,518 cm$^{-1}$ assigned to the C–H bending of the imidazolium group (Fig. 1e). The absorption bands at 562, 1,000–1,150, 1,653 and 2,850–3,000 cm$^{-1}$ are in correspondence with

vibrations of Fe–O, Si–O–Si, C=O and C–H stretching in Fe3O4@SiO2–polymer-imid–Pd (Fig. 1f). It also shows a band in the region of 790 cm$^{-1}$ which confirms the presence of C–Pd absorption frequency in Fe3O4@SiO2–polymer-imid–Pd (Fig. 1f).

Structural investigation of samples was carried out by powder X-ray diffraction (XRD) technique. Figure 2 shows the XRD patterns for pure $Fe_3O_4$, $Fe_3O_4@SiO_2$ and $Fe_3O_4@SiO_2$-polymer–Pd nanoparticles. As shown in Fig. 2a, the $Fe_3O_4$ nanoparticle has highly crystalline cubic spinel structure, which agrees with the standard $Fe_3O_4$ (cubic phase) XRD spectrum (PDF#88-0866). The characteristic peaks at $2\Theta = 30.1°$, 35.4°, 43.1°, 53.4°, 57° and 62.6° for pure $Fe_3O_4$ nanoparticles, which were marked, respectively, by their indices (220), (311), (400), (422), (511) and (440), were also observed for $Fe_3O_4@SiO_2$ and $Fe_3O_4@SiO_2$-polymer–Pd nanoparticles (reference JCPDS card no.19-629). This revealed that the surface modification and conjugation of the $Fe_3O_4$ nanoparticles do not lead to their phase change. From Fig. 2b, we can see the XRD pattern of $Fe_3O_4@SiO_2$ showing an obvious diffusion peak at $2\Theta = 15$–25°, generally considered as the diffusion peak of amorphous silica. For Fe3O4@SiO2–polymer-imid–Pd nanoparticles, the broad peak was transferred to lower angles due to the synergetic effect of amorphous silica and polymer. Also, the XRD pattern of Fe3O4@-SiO2–polymer-imid–Pd nanocatalyst, showing the peaks of both $Fe_3O_4$ and Pd and the diffraction peak at 39.79°, indicates that the Pd particles are in a metallic state. The
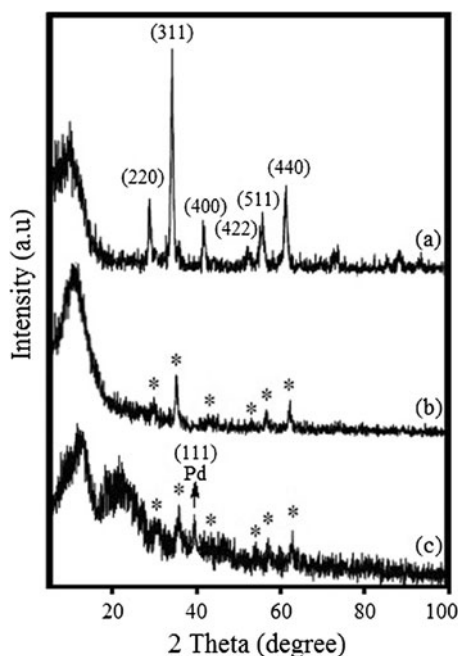
broadening of each peak in XRD mean crystallite size was calculated by applying Scherrer's equation: $D = 0.9 \ \lambda/\beta \cos\Theta$, where $D$ is the average diameter in A°, $\lambda$ is the wavelength of the X-rays, $\beta$ is the broadening of the diffraction line measured at half of its maximum intensity in radians and $\Theta$ is the Bragg diffraction angle. The mean crystallite size superparamagnetic nanocatalyst was found to be around 80 nm.

The morphology and sizes of (a) $Fe_3O_4$ and (b) $Fe_3O_4@SiO_2$ particles were observed by transmission electron microscopy (TEM) as shown in Fig. 3. As shown in Fig. 3a, the $Fe_3O_4$ nanoparticles prepared by the chemical coprecipitation are quasi spherical with an average of about 12 nm. Figure 1b clearly displays that $Fe_3O_4$ nanoparticles have been successfully encapsulated into the $SiO_2$ shell, and $Fe_3O_4@SiO_2$ nanoparticles were obtained with a diameter of about 20 nm due to the agglomeration of $Fe_3O_4$ inside nanospheres and surface growth of silica on the shell. The mesoporous silica shell on the surface of $Fe_3O_4$ is quite homogeneous and exhibits good monodispersity with an estimated thickness of 8 nm.

The morphology of Fe3O4@SiO2–polymer-imid–Pd nanoparticle was also observed by FE-SEM (Fig. 3c). The Fe3O4@SiO2–polymer-imid–Pd nanoparticles are spherical in shape with a smooth surface morphology. The diameter of the nanoparticles is found to be approximately 90 nm. The FE-SEM images indicate the successful coating of the magnetic $Fe_3O_4$ particles.

The hydrodynamic diameter of $Fe_3O_4$, $Fe_3O_4@SiO_2$ and Fe3O4@SiO2–polymer-imid–Pd nanoparticles is determined by the DLS technique (Fig. 3). This size distribution is centered at a value of 12, 20 and 85 nm for $Fe_3O_4$, $Fe_3O_4@SiO_2$ and Fe3O4@SiO2–polymer-imid–Pd, respectively (Fig. 3d–f). The theoretical curve of standard distribution from our studies was calculated by means of Microsoft Excel.

$N_2$ adsorption–desorption isotherm analysis provides information on the specific surface area and porosity of the prepared samples. The surface areas and average pore radius were measured by $N_2$ adsorption and results are shown in Table 1.

The results of magnetization measurements as a function of applied magnetic field are shown in Fig. 4a. It indicated that all products had superparamagnetism. The magnetization curve and demagnetization curve are coincident, no hysteresis phenomenon is found, and remanent magnetization and coercivity are equal to zero. As shown in Fig. 4a(a), the saturation magnetization of $Fe_3O_4$ is 65.8 emu/g, while for Fe3O4@SiO2–polymer-imid–Pd with a 75 nm shell 27.3 emu/g at 300 K [Fig. 4a(b)]. These results indicated that the magnetization of $Fe_3O_4$ decreased considerably with the increase of $SiO_2$ and polymer. Nevertheless, the polymer–Pd supported on $Fe_3O_4@SiO_2$



**Fig. 2** XRD patterns of a $Fe_3O_4$ [27], b $Fe_3O_4@SiO_2$ [27] and c Fe3O4@SiO2–polymer-imid–Pd
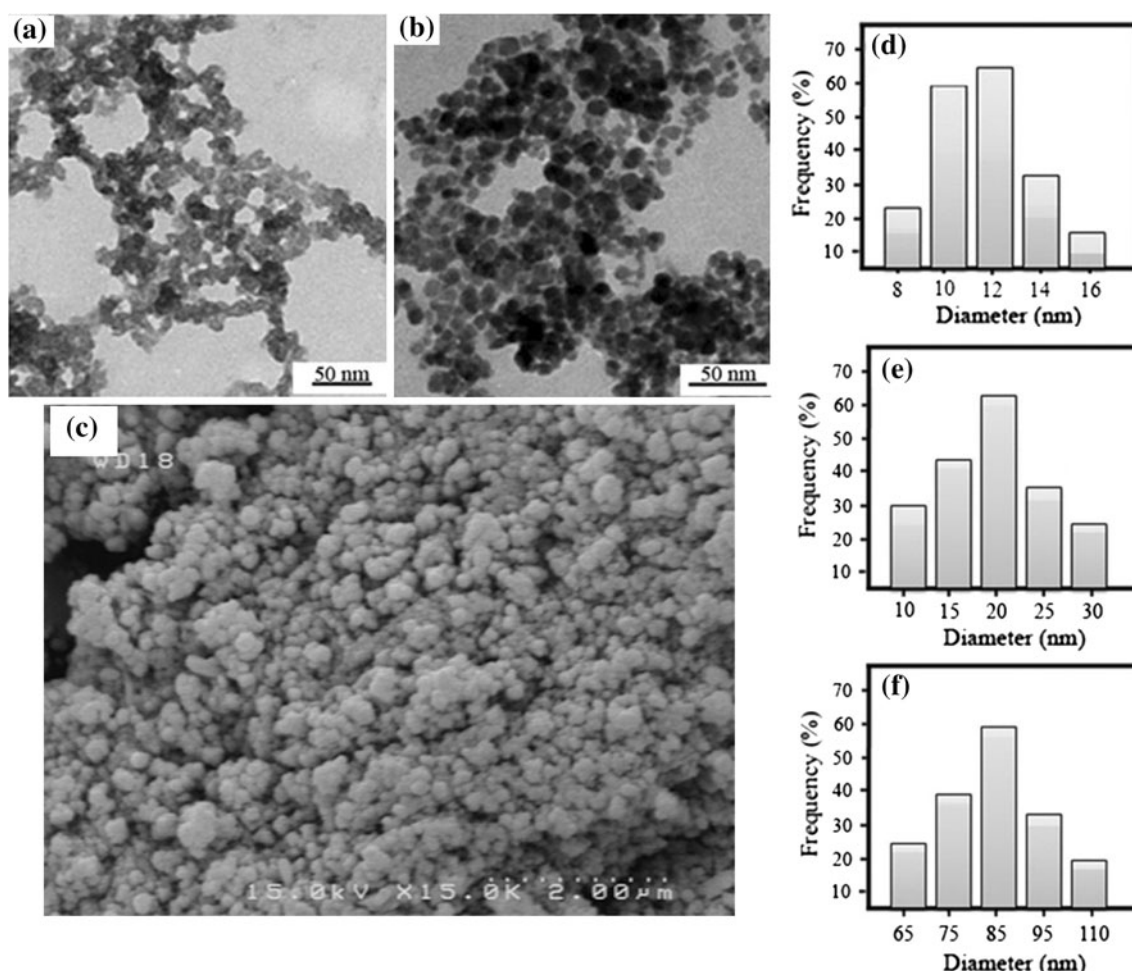
**Fig. 3** TEM and DLS images of Fe₃O₄ (**a**, **d**) [27], Fe₃O₄@SiO₂ (**b**), **e** [27] and FE-SEM and DLS images Fe3O4@SiO2–polymer-imid–Pd (**c**, **f**), respectively

**Table 1** BET result of Fe₃O₄, Fe₃O₄@SiO₂, Fe3O4@SiO2–polymer-imid–Pd and recovered catalysts[a]

| Catalyst/cycle reusability | Specific surface area (m²/g) | Pore volume (cm³/g) | Average pore radius (nm) |
| --- | --- | --- | --- |
| Fe₃O₄ | 480 | 0.803 | 1.254 |
| Fe₃O₄@SiO₂ | 350.3 | 0.755 | 1.787 |
| Cat. | 270 | 0.639 | 3.768 |
| Cat./first | 264 | 0.635 | 4.810 |
| Cat./second | 260 | 0.633 | 4.880 |
| Cat./third | 258 | 0.636 | 4.930 |
| Cat./fourth | 255 | 0.678 | 5.323 |
| Cat./fifth | 240 | 0.696 | 5.800 |

[a] Calculated by the BJH method

can still be separated from the solution by using an external magnetic field [Fig. 4a(b)].

Determination of Pd content was performed by inductively coupled plasma (ICP) analyzer. According to the ICP analysis, the Pd content in the magnetic nanocatalyst was determined, which revealed the presence of 0.33 mmol/g for this catalyst.

Thermal analysis was performed to confirm coating formation on the surface of Fe₃O₄@SiO₂. As shown in Fig. 4b, the TGA curve of Fe3O4@SiO2–polymer-imid–Pd shows first weight loss of 2.6 % below 120 °C, which might be due to the loss of adsorbed water in the sample. The mass loss of about 27.74 % by weight in the range of 200–500 °C is attributed to the decomposition of pure polymer and the temperature of the maximum weight loss is 487 °C (Fig. 4b). Below 200 °C, the rate of weight loss is relatively slow owing to the loss of residual water adhering to the sample surface. Thus, the TGA curve confirmed the successful grafting of polymer molecules on the magnetic surface.

The photographs of the dispersions of the Fe3O4@-SiO2–polymer-imid–Pd nanoparticles are given in Fig. 5a, which was well dispersed in DMF under normal conditions. On the contrary, the nanoparticles rapidly gathered
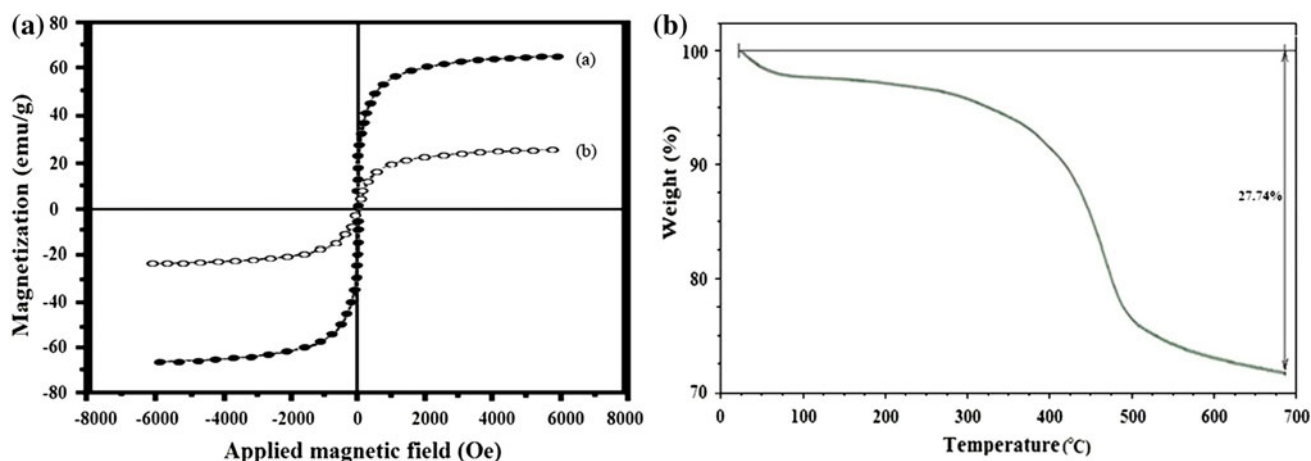
**Fig. 4** **a** Magnetization curves at 300 K for **a** Fe₃O₄ and **b** Fe3O4@SiO2–polymer-imid–Pd nanoparticles nanoparticles. **b** Thermogravimetric analysis of Fe3O4@SiO2–polymer-imid–Pd nanoparticles
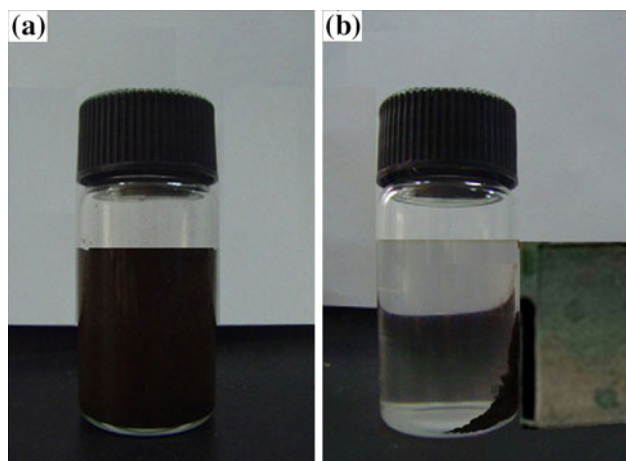


**Fig. 5** Catalyst ability for effective recovery at the end of reactions by an external magnetic field

on the sidewall of the cylinder under a magnetic approach (Fig. 5b). This result indicated that the Fe₃O₄@SiO₂-polymer–Pd nanoparticles can be easily manipulated by an external magnetic field.

To show the merit of application of these magnetic nanoparticles in organic synthesis, we applied them as the catalysts in the Sonogashira–Hagihara cross-coupling reactions. Initial studies were performed upon the reaction of iodobenzene with phenylacetylene as a model reaction and the effects of different solvents, temperature, bases and amount of catalyst were studied for this reaction (Table 2). To elucidate the role of the catalyst, initially the reaction between iodobenzene and phenylacetylene was examined in the presence of varying amounts of the nanocatalysts and the results are presented in Table 2. The best result was achieved by carrying out the reaction with (0.03 g:1:1.2 mmol) ratio of nanocatalyst, iodobenzene and phenylacetylene in DMF at 80 °C (Table 2, entry 6).

The use of a higher amount of nanocatalysts did not improve the yield (Table 2, entry 14), while a decrease in the amount of nanocatalysts decreased the yield (Table 2, entries 12 and 13). In the absence of a magnetic nanocatalyst, the reaction did not proceed even after a long reaction time (10 h) (Table 2, entry 17).

The results showed that among the tested solvents, DMF was more efficient and the desired product was obtained in shorter reaction times (30 min) and higher yields (Table 2, entry 6) than the other solvents under study (Table 2, entries 1–5). In the reactions employing tetrahydrofuran, toluene, water, acetonitrile and dimethyl sulfoxide as solvents, the reactions did not progress efficiently and after 2 h the desired product was obtained in only 66, 41, 79, 83 and 86 % yields, respectively, at 80 °C (Table 2, entries 1–5).

The effect of different bases on the reaction of iodobenzene (1 mmol) with phenylacetylene (1.2 mmol) in the presence of Fe₃O₄@SiO₂-polymer–Pd magnetic nanoparticles (0.03 g) in DMF (4 mL) at 80 °C was studied (Table 2, entries 6, 15-21). We have presented the results of this study in Table 2, which indicates that Et₃N is the most suitable among the different bases studied for this purpose (Table 2, entry 6).

Also, the effect of temperature was studied by carrying out the model reaction at different temperatures (room temperature, 40, 60, 80 and 90 °C) in DMF in the presence of Et₃N and the best results were obtained at 80 °C (Table 2, entries 6–10). Therefore, we continued the reactions under optimum conditions (Table 2, entry 6).

The generality of the reaction of phenylacetylene with diverse aryl halides was studied under optimum conditions, that is, Fe₃O₄@SiO₂-polymer–Pd (0.03 g), DMF (4 mL) and 2 mmol of Et₃N and the results are summarized in Table 3. As expected, the reaction of aryliodides bearing electron-donating groups was completed with longer

**Table 2** Optimization of different proportions of nanocatalyst and also effect of solvents, temperature and using different bases upon the reaction of iodobenzene with phenylacetylene as a model reaction[a]
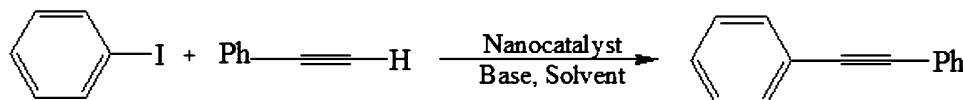


| Entry | Solvent | Catalyst amount (g) | Bases | Temperature (°C) | Yield[b] (%) |
|---|---|---|---|---|---|
| 1 | THF | 0.03 | $Et_3N$ | 80 | 66 |
| 2 | Toluene | 0.03 | $Et_3N$ | 80 | 41 |
| 3 | $H_2O$ | 0.03 | $Et_3N$ | 80 | 79 |
| 4 | $CH_3CN$ | 0.03 | $Et_3N$ | 80 | 83 |
| 5 | DMSO | 0.03 | $Et_3N$ | 80 | 86 |
| 6 | DMF | 0.03 | $Et_3N$ | 80 | 96 |
| 7 | DMF | 0.03 | $Et_3N$ | r.t | Trace |
| 8 | DMF | 0.03 | $Et_3N$ | 40 | 79 |
| 9 | DMF | 0.03 | $Et_3N$ | 60 | 84 |
| 10 | DMF | 0.03 | $Et_3N$ | 90 | 95 |
| 11 | DMF | –[c] | $Et_3N$ | 80 | – |
| 12 | DMF | 0.01 | $Et_3N$ | 80 | 22 |
| 13 | DMF | 0.02 | $Et_3N$ | 80 | 73 |
| 14 | DMF | 0.04 | $Et_3N$ | 80 | 95 |
| 15 | DMF | 0.03 | $Na_2CO_3$ | 80 | 23 |
| 16 | DMF | 0.03 | $K_2CO_3$ | 80 | 87 |
| 17 | DMF | 0.03 | $CS_2CO_3$ | 80 | 91 |
| 18 | DMF | 0.03 | NaOH | 80 | 64 |
| 19 | DMF | 0.03 | KOH | 80 | 66 |
| 20 | DMF | 0.03 | CsOH | 80 | 87 |
| 21 | DMF | 0.03 | DBU | 80 | 90 |

[a] Reactions were run in 4 ml solvent with 1 mmol iodobenzene, 1.2 mmol phenylacetylene and 2 mmol base for 2 h

[b] Isolated yield

[c] Time: 10 h

reaction times (Table 3, entries 2–4) than those with electron-withdrawing groups (Table 3, entries 5, 6, 8 and 9). The coupling of ortho- and meta-substituted iodobenzenes having ortho-methyl, ortho-chloro and meta-chloro groups took place with phenylacetylene to give the corresponding products in 87, 87, and 90 % yield, respectively (Table 3, entries 3, 8 and 9). The coupling reaction of phenylacetylene with both electron-releasing and electron-withdrawing aryl bromides afforded the desired products in high yields (Table 3, entries 10–17). Also, 3-bromopyridine, 5-bromopyrimidine and 2-thiophenyl iodide led to the corresponding arylated alkynes in good yields (Table 3, entries 15–17). Although aryl chlorides are not as reactive and are less likely employed in palladium-catalyzed coupling reactions, Sonogashira–Hagihara reactions could take place using phenylacetylene and aryl chlorides in the presence of catalytic amount of Fe3O4@SiO2–polymer-imid–Pd nanoparticles (Table 3, entries 18-21).

To confirm the reusability and stability of the magnetic nanocatalyst, it was separated from the reaction mixture after its first use in the Sonogashira–Hagihara reaction. The recovered catalyst was found to be reusable for six cycles with a slight loss in activity (Fig. 6).
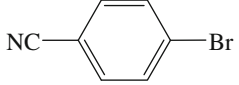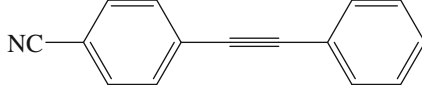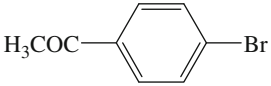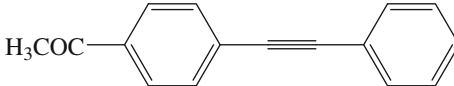
## Conclusions
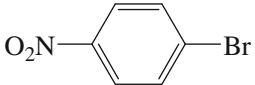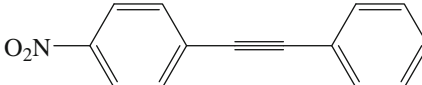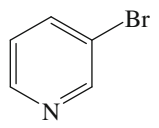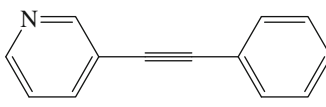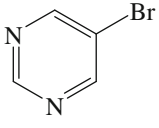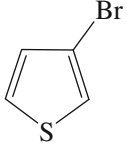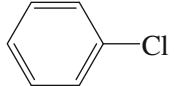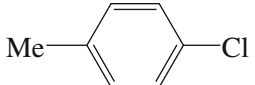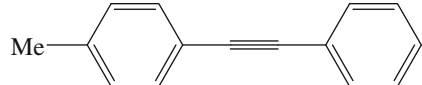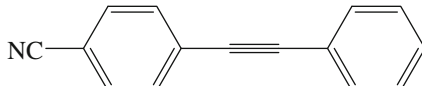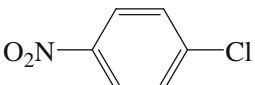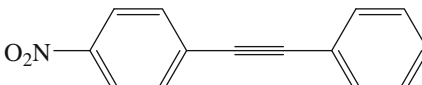
$Fe_3O_4$ was successfully prepared by co-precipitation with $FeCl_2$ and $FeCl_3$ as reaction substrate, polyvinyl alcohol (PVA 15000) as surfactant and hexamethylenetetraamine as precipitant. The core–shell $Fe_3O_4@SiO_2$ nanospheres were prepared by a modified Stober method. Then, $Fe_3O_4@SiO_2$ was coated with polymeric N-heterocyclic carbene/Pd. The nanocatalyst was successfully synthesized and structural, surface, morphological and magnetic properties of these nanoparticles were evaluated. TEM microscopy revealed a very fine layer of $SiO_2$ and polymer

**Table 3** Sonogashira–Hagihara coupling of different aryl halides with phenylacetylene in DMF in the presence of the catalyst using $Et_3N$ as a base[a]
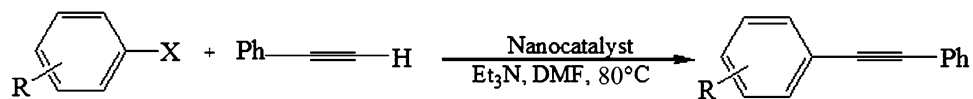
| Entry | Aryl halide | Product | Time (h) | Yield (%)[b] | References |
|-------|-------------|---------|----------|-------------|------------|
| 1 | | | 0.5 | 96 | [56] |
| 2 | | | 2.5 | 93 | [56] |
| 3 | | | 3 | 87 | [56] |
| 4 | | | 3 | 91 | [56] |
| 5 | | | 1.2 | 93 | [56] |
| 6 | | | 1.5 | 94 | [56] |
| 7 | | | 3 | 90 | [56] |
| 8 | | | 2 | 87 | [57] |
| 9 | | | 1.5 | 90 | [57] |
| 10 | | | 2 | 93 | [56] |
| 11 | | | 4 | 90 | [56] |

**Table 3** continued

| Entry | Aryl halide | Product | Time (h) | Yield (%)[b] | References |
|-------|-------------|---------|----------|--------------|------------|
| 12 | NC—⟨ ⟩—Br | NC—⟨ ⟩—≡—⟨ ⟩ | 3 | 92 | [56] |
| 13 | H₃COC—⟨ ⟩—Br | H₃COC—⟨ ⟩—≡—⟨ ⟩ | 3 | 92 | [56] |
| 14 | O₂N—⟨ ⟩—Br | O₂N—⟨ ⟩—≡—⟨ ⟩ | 2.5 | 93 | [56] |
| 15 | pyridine-Br | pyridine-≡—⟨ ⟩ | 3 | 91 | [56] |
| 16 | pyrimidine-Br | pyrimidine-≡—⟨ ⟩ | 3 | 92 | [56] |
| 17 | thiophene-Br | thiophene-≡—⟨ ⟩ | 4 | 89 | [56] |
| 18 | ⟨ ⟩—Cl | ⟨ ⟩—≡—⟨ ⟩ | 7 | 78 | [56] |
| 19 | Me—⟨ ⟩—Cl | Me—⟨ ⟩—≡—⟨ ⟩ | 10 | 76 | [56] |
| 20 | NC—⟨ ⟩—Cl | NC—⟨ ⟩—≡—⟨ ⟩ | 4 | 87 | [58] |
| 21 | O₂N—⟨ ⟩—Cl | O₂N—⟨ ⟩—≡—⟨ ⟩ | 3 | 90 | [56] |

[a] Reactions were performed with ArX (1 mmol), phenylacetylene (1.2 mmol) and Et₃N (2 mmol) catalyst (0.03 g) in DMF (4 mL) at 80 °C

on the $Fe_3O_4$. The size of the prepared nanoparticles with roughly spherical shapes and core–shell structures was about 20 nm in diameter. Moreover, magnetization curves demonstrated a high degree of superparamagnetism. Magnetic nanocatalyst with saturation magnetization value of about 27.3 emu/g can be readily recovered under an external magnetic field. The amount of polymer capsulated around the magnetite nanoparticles in the prepared magnetic nanocatalyst was estimated to be 27.74 % by weight. The crystallite size obtained from X-ray line profile fitting is comparable with the particle size obtained from TEM.

Therefore, considering the importance of this catalyst, we have shown that Fe3O4@SiO2–polymer-imid–Pd is an efficient and stable nanocatalyst and is strongly active in coupling reactions of aryl halides with terminal alkynes. This method gives notable advantages such as easy preparation, heterogeneous nature and easy separation of the catalyst by external magnetic field, excellent yields, short reaction times and simplicity of operation, making it a facile tool in the Sonogashira–Hagihara cross-coupling reaction. In addition, the novel catalyst used is easily recovered by using a permanent magnet and reused without
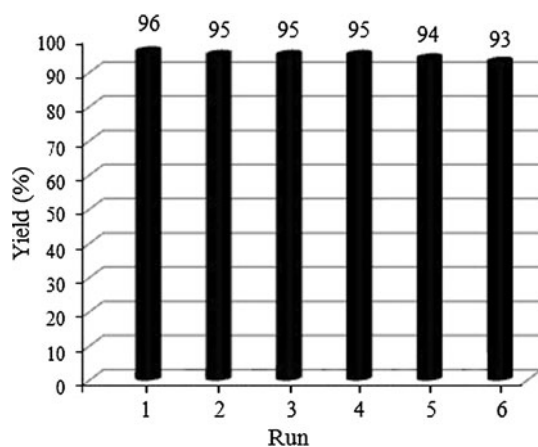
**Fig. 6** Recycling of the catalyst for the reaction of iodobenzene with phenylacetylene in the presence of $Et_3N$. Reaction conditions: iodobenzene (1 mmol), phenylacetylene (1.2 mmol), catalyst (0.03 g), $Et_3N$ (2 mmol), in DMF (4 mL) at 80 °C

any noticeable loss of activity after at least six times. The formation of the carbene–Pd bond leads to leaching of reduced Pd nanoparticles. Polymer chains acts as spacer between Fe3O4@SiO2 and Pd and leads to the increased catalytic activity of Pd. The ICP analysis does not show any Pd leaching at this stage. This experiment confirmed the heterogeneous character of the catalytically active species.

## References

1. C.C. Koch, *Nanostructured materials, processing, properties and applications* (Norwich, New York, 2002)
2. J.M. Cowley, *Diffraction physics* (North-Holland, New York, 1981)
3. J.M. Cowley, Appl. Phys. Lett. **15**, 58 (1969)
4. J.M. Cowley, Ultramicroscopy. **49**, 4 (1993)
5. E. Zeitler, M.G.R. Thomson, Optik. **31**, 258 (1970)
6. J.M. Rodenburg, R.H.T. Bates, Philos. Trans. R. Soc. **339**, 521 (1992)
7. D. Zanchet, B.D. Hall, D. Ugarte, *Characterization of nanophase materials* (Wiley, Germany, 2000)
8. E.W. Wong, M.J. Bronikowski, M.E. Hoenk, R.S. Kowalczyk, B.D. Hunt, Chem. Mater. **17**, 237 (2005)
9. M.M. Miller, G.A. Prinz, S.F. Cheng, S. Bounnak, Appl. Phys. Lett. **81**, 2211 (2002)
10. S. Sun, C.B. Murray, D. Weller, L. Folks, A. Moser, Science. **287**, 1989 (2000)
11. M.M.J. Modo, J.W.M. Bulte, *Molecular and cellular MR imaging* (CRC Press, Boca Raton, 2007)
12. C. Burtea, S. Laurent, A. Roch, L. Vander Elst, R.N. Muller, J. Inorg. Biochem. **99**, 1135 (2005)
13. J.W. Bulte, Methods Mol. Med. **124**, 419 (2006)
14. S. Boutry, S. Laurent, L. Vander Elst, R.N. Muller, Contrast Med. Mol. Imaging. **1**, 15 (2006)
15. I. Chourpa, L. Douziech-Eyrolles, L. Ngaboni-Okassa, J.F. Fouquenet, S. Cohen-Jonathan, M. Souce, H. Marchais, P. Dubois, Analyst. **130**, 1395 (2005)
16. J. Javidi, M. Esmaeilpour, Colloid. Surface B. **102**, 265 (2013)
17. S.W. Charles, J. Popplewell, Endeavour. **6**, 153 (1982)
18. A.K. Gupta, M. Gupta, Biomaterials. **26**, 3995 (2005)
19. H. Pardoe, P.R. Clark, T.G. St Pierre, P. Moroz, S.K.A. Jones, Magn. Reson. Imag. **21**, 483 (2003)
20. L. Lei, X. Liu, Y. Li, Y. Cui, Y. Yang, G. Qin, Mater. Chem. Phys. **125**, 866 (2011)
21. B. Sahoo, S.K. Sahu, P. Pramanik, J. Mol. Catal. B Enzym. **69**, 95 (2011)
22. K. Suslick, M. Fang, T. Hyeon, J. Am. Chem. Soc. **118**, 11960 (1996)
23. S. Veintemillas-Verdaguer, M.P. Morales, C.J. Serna, Mater. Lett. **35**, 227 (1998)
24. P. Tartaj, C. Serna, Chem. Mater. **14**, 4396 (2002)
25. D. Kim, Y. Zhang, W. Voit, K. Rao, M. Muhammed, J. Magn. Magn. Mater. **225**, 30 (2001)
26. R. Massart, E. Dubois, V. Cabuil, E. Hasmonay, J. Magn. Magn. Mater. **149**, 1 (1995)
27. M. Esmaeilpour, A.R. Sardarian, J. Javidi, Appl. Catal. A **445–446**, 359 (2012)
28. K. Ohno, K.M. Koh, Y. Tsujii, T. Fukuda, Macromolecules. **35**, 8989 (2002)
29. S. Sun, S. Anders, H.F. Hamann, J.U. Thiele, J.E.E. Baglin, T. Thomson, E.E. Fullerton, C.B. Murray, B.D. Terris, J. Am. Chem. Soc. **124**, 2884 (2002)
30. P.D. Stevens, J. Fan, H.M.R. Gardimalla, M. Yen, Y. Gao, Org. Lett. **7**, 2085 (2005)
31. S. Shylesh, V. Schunemann, W.R. Thiel, Angew. Chem. Int. Ed. **49**, 3428 (2010)
32. A. Schatz, M. Hager, O. Reiser, Adv. Funct. Mater. **19**, 2109 (2009)
33. V. Polshettiwar, R. Luque, A. Fihri, H. Zhu, M. Bouhrara, J.M. Basset, Chem. Rev. **111**, 3036 (2011)
34. A. Schatz, O. Reiser, W.J. Stark, Chem. Eur. J. **16**, 8950 (2010)
35. K. Sonogashira, Y. Tohda, N. Hagihara, Tetradron. Lett. **16**, 4467 (1975)
36. R. Chinchilla, C. Najera, Chem. Rev. **107**, 874 (2007)
37. I. Paterson, R.D.M. Davies, R. Marquez, Angew. Chem. Int. Edit. **40**, 603 (2001)
38. G. Amiet, H.M. Hugel, F. Nurlawis, Synlett. **41**, 495 (2002)
39. N.D.P. Cosford, L. Tehrani, J. Roppe, E. Schweiger, M. Washburn, M.A. Varney, J. Med. Chem. **46**, 204 (2003)
40. P. Li, L. Wang, H. Li, Tetrahedron. **61**, 8633 (2005)
41. G. Altenhoff, S. Wurtz, F. Glorius, Tetrahedron Lett. **47**, 2925 (2006)
42. A. Nagy, Z. Nova'k, A. Kotschy, J. Organomet. Chem. **690**, 4453 (2005)
43. F. Yang, X. Cui, Y. Li, J. Zhang, G. Ren, Y. Wu, Tetrahedron. **63**, 1963 (2007)
44. M. Cai, Q. Xu, J. Sha, J. Mol. Catal. A Chem. **272**, 293 (2007)
45. M.B. Thathagar, G. Rothenberg, Org. Biomol. Chem. **4**, 111 (2006)
46. K.R. Reddy, N.S. Kumar, P.S. Reddy, B. Sreedhar, M.L. Kantam, J. Mol. Catal. A Chem. **252**, 12 (2006)
47. J. Ruiz, N. Cutillas, F. Lopez, G. Lopez, D. Bautista, Organometallics. **25**, 5768 (2006)
48. C. Yi, R. Hua, J. Org. Chem. **71**, 2535 (2006)
49. Y. Liang, Y.X. Xie, J.H. Li, J. Org. Chem. **71**, 379 (2006)
50. L. Feng, F. Liu, P. Sun, J. Bao, Synlett. **10**, 1415 (2008)
51. X. Xie, X. Xu, H. Li, X. Xu, J. Yang, Y. Li, Adv. Synth. Catal. **351**, 1263 (2009)

52. M. Carril, A. Correa, C. Bolm, Angew. Chem. Int. Ed. **47**, 4862 (2008)
53. M. Bakherad, A. Keivanloo, S. Mihanparast, Synth. Commun. **40**, 179 (2010)
54. H.N. Borah, D. Prajapati, R.C. Boruah, Synlett. **655**, 2823 (2005)
55. S. Park, M. Kim, D.H. Koo, S. Chang, Adv. Synth. Catal. **346**, 1638 (2004)
56. H. Firouzabadi, N. Iranpoor, M. Gholinejad, J. Mol. Catal. A Chem. **321**, 110 (2010)
57. T. Suzuka, Y. Okada, K. Ooshiro, Y. Uozumi, Tetrahedron. **66**, 1064 (2010)
58. H. Firouzabadi, N. Iranpoor, F. Kazemi, M. Gholinejad, J. Mol. Catal. A Chem. **357**, 154 (2012)